Supplementary Information

Bifunctional nanoporous gold-copper@ZIF film for highly efficient nitrogen electro-fixation

Shulin Zhao[1], Guorui Tang[1], Xiaoyun Liu[1], Yue Pang[1], Yijie Yang[1]*, Cheng-Peng Li[1]*

Table of Contents

Section S1 Experimental.

1. Materials

Sodium nitroferricyanide(Ⅲ) dihydrate ($C_5H_4FeN_6Na_2O_3$, 99.98%), salicylic acid ($C_7H_6O_3$, 99.5%) and sodium hypochlorite (NaClO, 6-14% active chlorine basis) were purchased in Ron Reagent. N,N-dimethylformamide ($HCON(CH_3)_2$, ≥99.5%) and sodium hydroxide (NaOH, 96%) were purchased in Tianjin Kemiou Chemical Reagent Co., Ltd. Potassium nitrate (KNO_3, ≥99.0%) was purchased from Tianjin North Tianyi Chemical Reagent Factory. Trisodium citrate dihydrate ($C_6H_5Na_3O_7 \cdot 2H_2O$, 99%) was purchased from Tianjin Damao Chemical Trading Co., Ltd. Potassium hydroxide (KOH, 96%) were purchased from Tianjin Yuanli Chemical Co., Ltd. Acetone (CH_3COCH_3, ≥99.5%), isopropyl alcohol ($(CH_3)_2CHOH$, ≥99.5%), ethylene glycol ($HOCH_2CH_2OH$), concentrated hydrochloric acid (36.0-38.0%) and sodium sulfate anhydrous (Na_2SO_4, 99%) were obtained from Tianjin Wind Ship Chemical Reagent Co., Ltd. Sulfamic acid (H_3NO_3S, 99.5%), ascorbic acid (AA, > 99.0%), gold chloride solution (Au 23.5 ~ 23.8% in dilute HCl), potassium bromide (KBr, photographic primary), Ammonium chloride (NH_4Cl, 99.99%), 1-propanethiol (C_3H_8S, 98%), 1-dodecanethiol ($C_{12}H_{26}S$, 98%) and zinc acetate dihydrate ($C_4H_6O_4Zn \cdot 2H_2O$, 99.995%) were obtained from Aladdin. Ethanol absolute (CH_3CH_2OH, ≥99.7%) was purchased from Shandong Bocheng Chemical Co., Ltd. Polyethylene pyrrolidone (PVP, average M.W. = 130,000, 99%) was from Shanghai Yuanye Bio-Technology Co., Ltd. Copper sultate pentahydrate ($CuSO_4 \cdot 5H_2O$, 99.8%), 1-hexanethiol ($C_6H_{14}S$, 96%) and nafion dispersion solution de1021 cs type (~5% in a mixture of lower aliphatic alcohols and water) were purchased from Shanghai Meryer Biochemical Technology Co., Ltd. 4-(Dimethylamino)benzaldehyde ($C_9H_{11}NO$, 99.97%) and 4,5-dichloroimidazole ($C_3H_2Cl_2N_2$, 98%) were from Bide Pharmatech Co., Ltd. Hydrazine hydrate (N_2H_4, 5%

HCl) was obtained from Guobiao (Beijing) Testing and Certification, Co., Ltd. 1H,1H,2H,2H-Perfluorodecanethiol ($CF_3(CF_2)_7CH_2CH_2SH$, 97%) were obtained from was obtained from Shanghai Macklin Biochemical Co., Ltd. All chemical reagents were used without further purification.

Scanning electron microscopy (SEM) images were obtained with a JSM-6700F (JEOL) operating at 5 kV in LABE mode. Transmission electron microscopy (TEM) imaging was performed on a Philips Tecnai F20 system at 200 kV to observe the morphology and quantitatively and qualitatively analyze the elements by EDS mapping. A ethanol absolute of materials was drop-casted on silica substrate and dried for static contact angle measurement, which was performed on a Lauda Scientific LSA100 equipped with the Firewire digital camera. The static contact angle was measured with an ultrapure water droplet (3 μL). Each result was averaged by three tests taken on the materials functionalized silica substrate. At the same time, the nitrogen contact angle test in water is carried out in nitrogen. The silicon wafer with the material was immersed in water and the contact angle of the material to nitrogen was tested using Lauda Scientific LSA100. Powder X-ray diffraction (XRD) patterns were recorded on a SmartLab-SE XRD diffractometer with Cu Kα radiation to obtain the structures of composites. The chemical composition and bonding characteristics were analyzed by X-ray photoelectron spectroscopy (XPS) of PHI Quantera under monochromatic Mg X-ray radiation source. Use of Micromeritics AutoChem II 2920, under the environment of nitrogen to Temperature Programmed Desorption materials (TPD) test. Fourier infrared spectroscopy (FTIR) testing of the materials was performed in the Thermo Scientific Nicolet iS20 instrument.

2. Synthesis of materials for comparison

Synthesis of AuNPs. AuNPs materials were initiated by the addition of 9.3 μL of $HAuCl_4$ solution to a round-bottomed flask containing 100 mL of solution. The mixture was then stirred thoroughly and heated to boiling. 10 mL (51 mg) of an aqueous trisodium citrate solution were added, resulting in a change from colorless to burgundy in the solution. After 10 minutes of heating with stirring, the solution

was cooled to room temperature. The resulting product was collected by centrifugation and washed several times with methanol, then dried under vacuum for 6 hours to finally obtain AuNPs (solid).

Synthesis of AuNPs/C_6. AuNPs materials were dispersed in the solvent of 1-mL ethanol and 1-mL IPA with the addition of 1.4-mL hexanethiol solution (0.6 mM). After 4-h reaction, products were collected by centrifugation and then dispersed in the solvent of 1-mL ethanol and 1-mL IPA. Then the above step was repeated and the final product was subjected to vacuum drying.

Synthesis of AuNPs/C_6@ZIF-71. 5-mg AuNPs/C_6 alloy materials were dispersed in 1 mL of ethanol. AuNPs/C_6 catalyst solution (6 μL, 5 mg/mL) was dropped on the surface of the polished glassy carbon electrode and naturally dried at room temperature. The electrode is immersed in the solution (the solution contained 0.125-mL DMF, 0.375-mL methanol, 0.250-mL 0.2 M zinc acetate dihydrate and 0.250-mL 0.4 M 4,5-dichloroimidazole). The electrodes were rinsed several times with methanol after 40 minutes.

Synthesis of CuNP.: Synthetic protocol of CuNPs materials were analogous to that of NP-AuCu structures. A round-bottomed flask was used to mix 50 mg of PVP and 450 mg of AA. Subsequently, 8 mL of EG was added and the mixture was stirred for 10 minutes. Subsequently, the round-bottomed flask was transferred to an oil bath and heated to 85 °C. A solution of 2 mL (3.6 mg) of $CuSO_4$ was then added to the flask, resulting in a change from colorless to pink. Following a 30-minute heating period at 85 °C, 2-mL (375 mg) KBr solution was added. After 90 minutes, the solution was cooled to room temperature. The product was collected by centrifugation and washed several times with ethanol and acetone to remove any remaining precursors and by-products. After vacuum drying for 6 hours, CuNPs were obtained.

Synthesis of CuNPs/C_6. CuNPs materials were dispersed in the solvent of 1-mL ethanol and 1-mL IPA with the addition of 1.4-mL hexanethiol solution (0.6 mM). After 4-h reaction, products were collected by centrifugation and then dispersed in the solvent of 1-mL ethanol and 1-mL IPA. Then the above step was

repeated and the final product was subjected to vacuum drying.

Synthesis of CuNPs/C_6@ZIF-71. 5-mg CuNPs/C_6 alloy materials were dispersed in 1 mL of ethanol. CuNPs/C_6 catalyst solution (6 μL, 5 mg/mL) was dropped on the surface of the polished glassy carbon electrode and naturally dried at room temperature. The electrode is immersed in the solution (the solution contained 0.125-mL DMF, 0.375-mL methanol, 0.250-mL 0.2 M zinc acetate dihydrate and 0.250-mL 0.4 M 4,5-dichloroimidazole). The electrodes were rinsed several times with methanol after 40 minutes.

3. Electrochemical measurements

Electrochemical tests were made using he electrochemical station (CHI760E) with three-electrode system. NP-AuCu/C_6@ZIF-71 were used as the working electrode, Ag/AgCl as the reference electrode, and Pt sheet as the counter electrode for electrolysis in an electrolytic cell. For NOR electrochemical testing, a gas-tight, two-compartment cell separated by a Nafion membrane was used for evaluation. The working electrode and the Ag/AgCl reference electrode were placed in the cathode chamber. In the anode chamber, a graphite plate was used as the counter electrode. Before the experiment, the membrane was boiled in ultrapure water for 1-hour, treated in H_2O_2 (5%) aqueous solution at 80 ℃ for 1-h. Then, the membrane was soaked in 0.5 M H_2SO_4 for 2-h at 80 ℃, and subsequently boiled in water for 6-h.

Before experiment, the electrolyte (0.1 M Na_2SO_4 for NRR, 0.1 M KOH for NOR) in the cathode cell was bubbled with pretreated N_2 for at least 1-h to ensure that air was excluded in the electrolyte. All given potentials were converted to reversible hydrogen electrode potential by E(vs RHE) = E(vs Ag/AgCl) + 0.059 pH + 0.197 V. The constant and stable access of N_2 is maintained during the electrolysis process.

4. Detection of ammonia

Ammonia in the electrolyte was quantified after 2-h electrolysis by indophenol blue method. Firstly, the color reagent system were prepared. Solution A: 1 M NaOH solution (containing 5% salicylic acid and 5% trisodium citrate); solution B: 0.05 M

NaClO solution; solution C: 1 wt% $C_5FeN_6Na_2O$ (sodium nitroferricyanide) aqueous solution. 2-mL of electrolyte was mixed with 2-mL solution A, 1-mL solution B and 0.2-mL solution C evenly, and the reaction was kept for 2-h at room temperature. The absorbance at 655 nm was recorded by using a UV-Vis absorption spectrometer. Next, NH_4Cl standard solution with a series of different concentrations was configured for UV-Vis tests and the standard curve of indophenol blue method was drawn to detect ammonia. The ammonia concentration in the electrolyte was calculated by the linear equations.

5. Detection of nitrate

5-mL of electrolyte was taken out of the electrolytic cell after 10-h electrolysis. Then, 0.1-mL 1 M HCl and 0.01-mL 0.8 wt% sulfamic acid solution were added to the aforementioned solution. The absorption spectrum was tested using an ultraviolet-visible spectrophotometer and the absorption intensities at wavelengths of 220 and 275 nm were recorded. The final absorbance value was calculated by the equation:

$$A = A_{220\,nm} + 2A_{275\,nm}$$

The concentration-absorbance curve was calibrated using a series of standard potassium nitrate solutions and the potassium nitrate crystal was dried at 105-110 ℃ for 2-h in advance.

6. Detection of hydrazine

The by-product N_2H_4 in the electrolyte was quantified after 2-h electrolysis by Watt-Chrisp method. Firstly, the color reagent system was prepared. P-dimethylaminated benzaldehyde (5.99 mg) was dissolved in a mixture of absolute ethanol (300 mL) and concentrated hydrochloric acid (30 mL). 5-mL of chromogen was mixed with 5 mL of electrolyte and kept at room temperature for 20-min. The absorbance at 455 nm was recorded by using a UV-Vis absorption spectrometer. Then, a series of concentrations of N_2H_4 standard solution was tested by UV-Vis to established the standard curve of N_2H_4. The hydrazine concentration in the electrolyte was calculated by the linear equations.

7.Detection of nitrite

The by-product nitrite in the electrolyte was quantified after 10-h electrolysis by Watt-Chrisp method. First, Griess reagent was prepared from 0.1 g N-(1-naphthyl) ethylenediamine dihydrochloride, 1.0 g sulfonamide and 2.94 mL H_3PO_4 dissolved in 50 mL deionized water. Then, the 1.0 mL Griess reagent was mixed with 1.0 mL electrolyte and 2.0 mL H_2O and reacted at room temperature for 10 min, where sulfanilamide reacted with NO_2^- to form a diazo salt and then further reacted with the amine to form an azo dye. Next, a series of concentrations of standard solutions were prepared, and the absorbance at 540 nm was measured by UV-Vis to quantify the concentration of NO_2^-.

8. Calculation of yield rate and Faradaic efficiency

The performance of catalysts mainly depends on their high catalytic activity, high selectivity and excellent stability. The high catalytic activity can be measured by the Faradaic efficiency and yield rate. Faradaic efficiency refers to the ratio of the charge consumed in the electrocatalytic synthesis to the total charge passing through the electrode, which can be calculated according to the following equation:

$$FE_{\mathrm{eNRR}} = \frac{3 \times F \times C_{NH_3} \times V}{Q}$$

$$FE_{\mathrm{eNOR}} = \frac{5 \times F \times C_{NO_3^-} \times V}{Q}$$

The NH_3 yield rate can be calculated by using the following equation:

$$\upsilon_{NH3} = \frac{C_{NH_3} \times V}{\mathrm{t} \times A_{\mathrm{cat.}}}$$

where F is Faraday's constant, C_{NH_3} is the ammonia concentration determined by indophenol blue method, V is the electrolyte volume of NRR, Q is the quantity of applied electricity, t is the time of electrochemical reaction, and $A_{cat.}$ is the area covered by the catalyst.

The NO_3^- yield rate can be calculated by using the following equation:

$$\upsilon_{NO_3^-} = \frac{C_{NO_3^-} \times V}{t \times A_{cat.}}$$

where F is Faraday's constant, $C_{NO_3^-}$ is the nitrate concentration determined by indophenol blue method, V is the electrolyte volume of NOR, Q is the quantity of applied electricity, t is the time of electrochemical reaction, and $A_{cat.}$ is the area covered by the catalyst.

Section S2 Characterization of Materials.

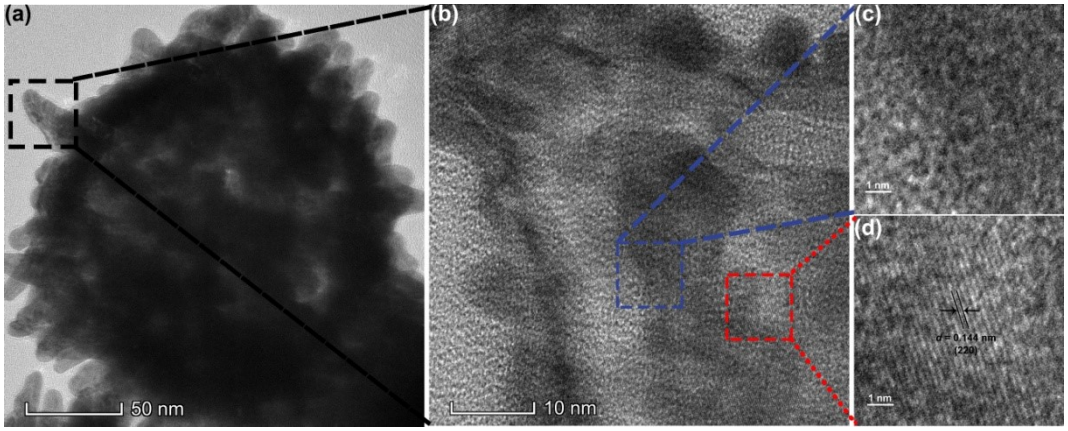

Figure S1. (a) TEM image of NP-AuCu and (b-d) high-resolution TEM image in the square area. The lattice structure of Au shows plane spacing of 0.144 nm, which is indexed to the (220) lattice plane.

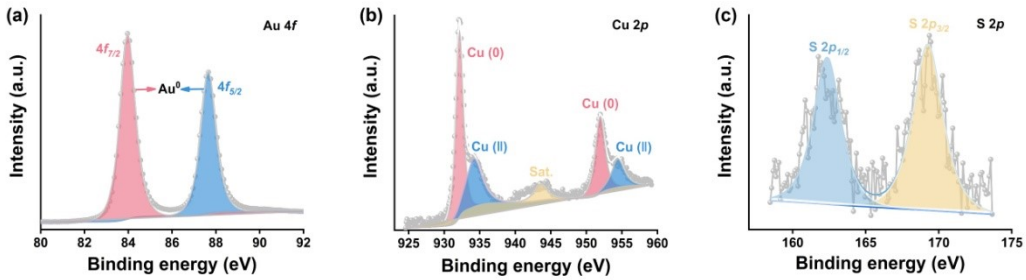

Figure S2. XPS at (a) Au 4*f*, (b) Cu 2*p* and (c) S 2*p* binding energy windows for NP-AuCu/C_6.

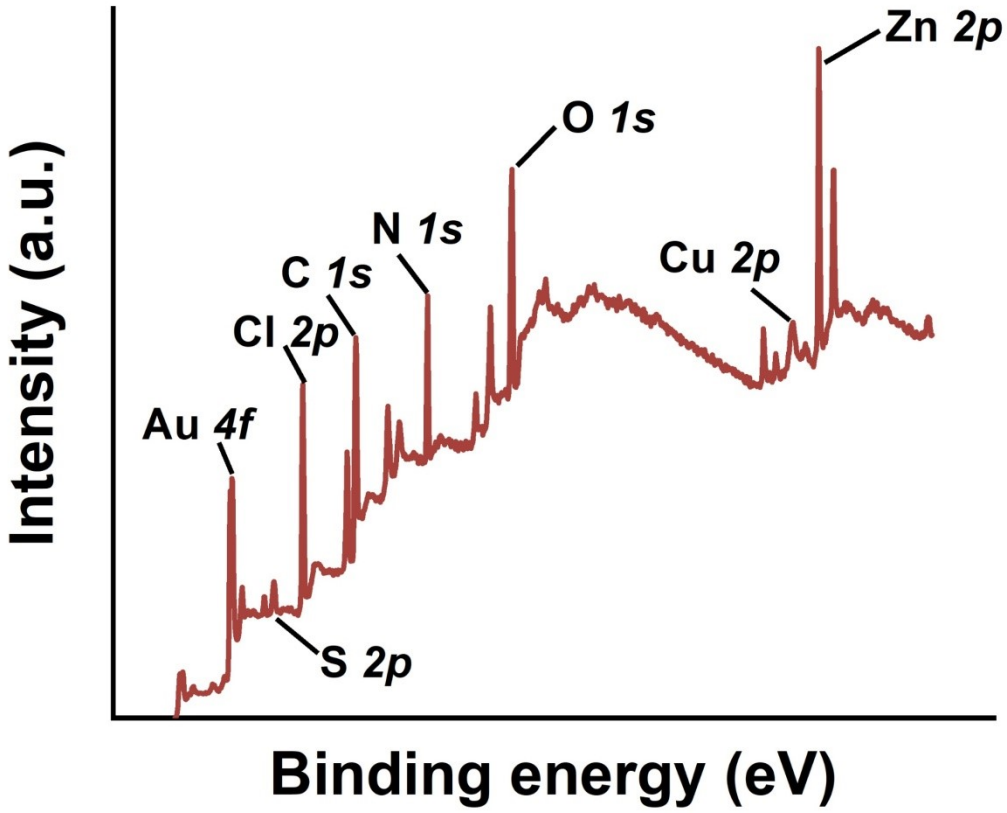

Figure S3. X-ray photoelectron spectroscopy (XPS) survey spectrum of NP-AuCu/C_6@ZIF-71.

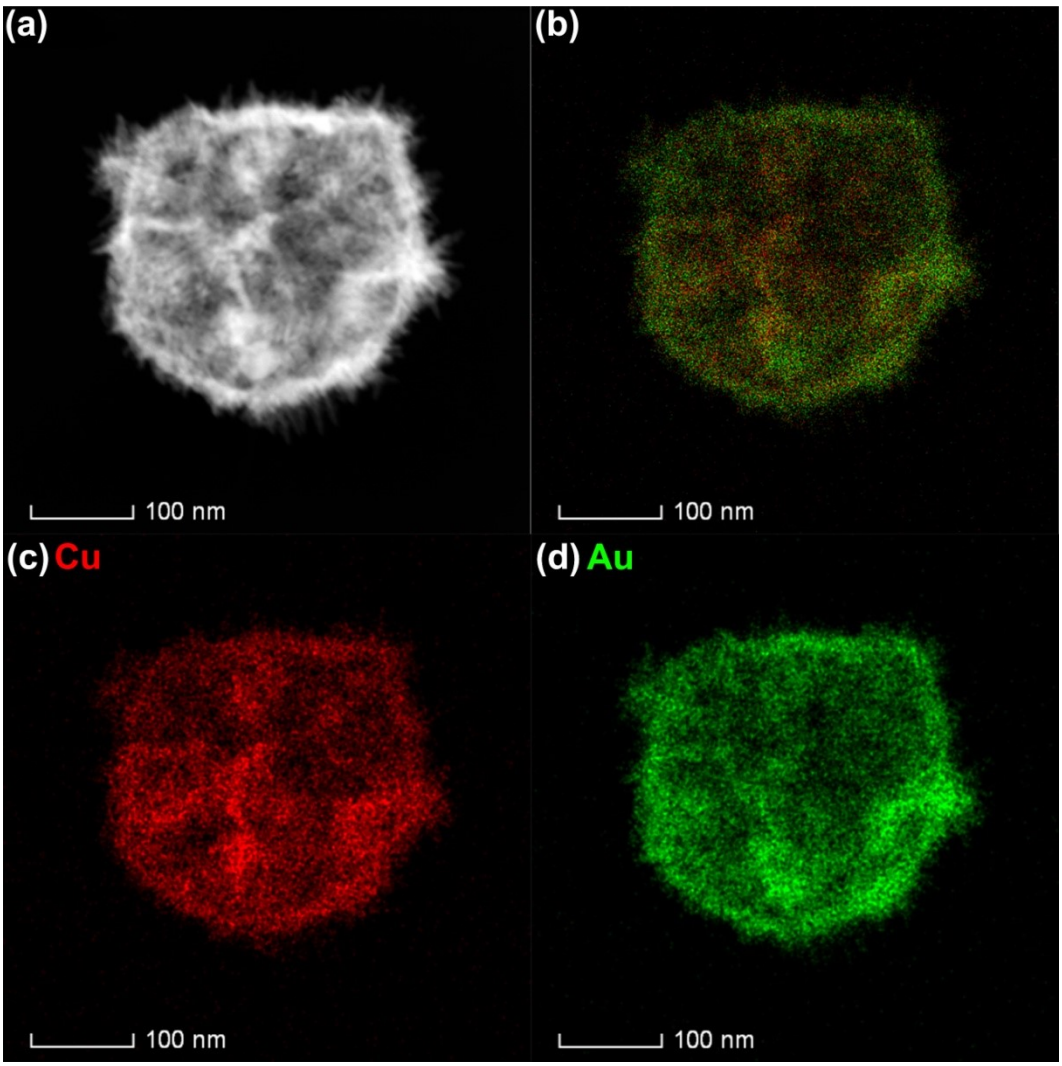

Figure S4. (a) The corresponding HAADF-STEM image of NP-AuCu (scale bar: 100 nm). And (b-d) is elemental mapping images of NP-AuCu. The Au:Cu atomic ratio of NP-AuCu is 46:54.

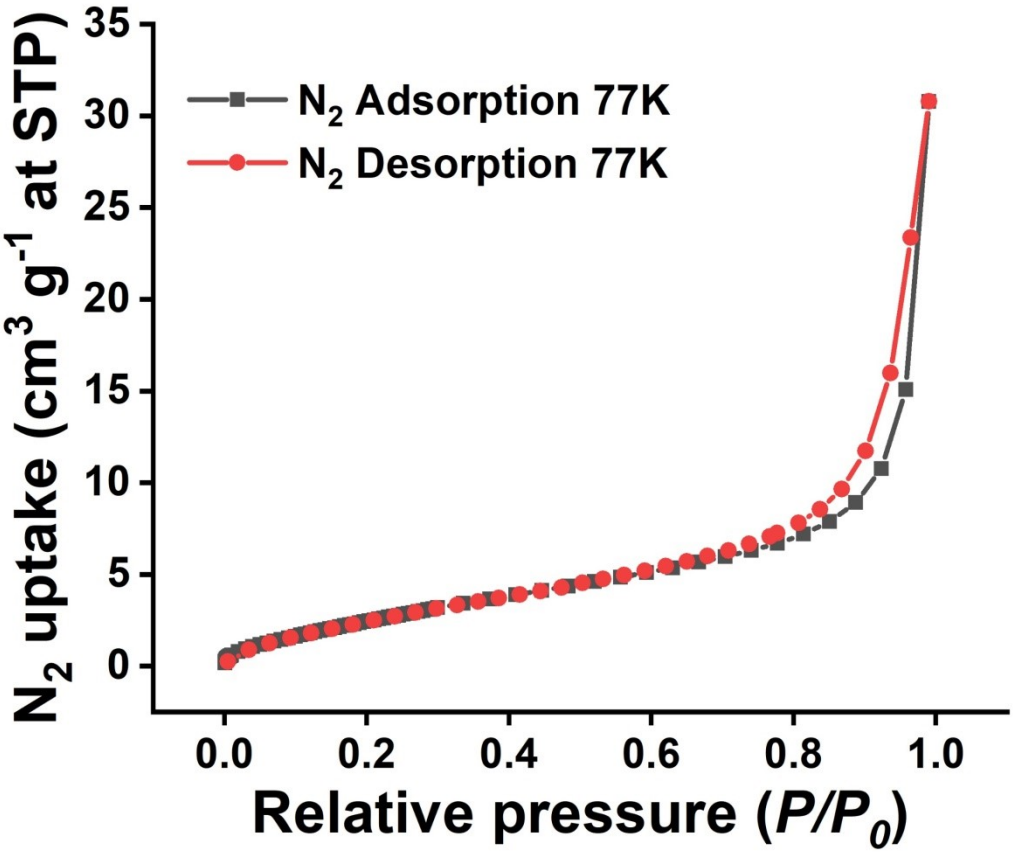

Figure S5. Nitrogen-sorption isotherms of NP-AuCu structure at 77 K.

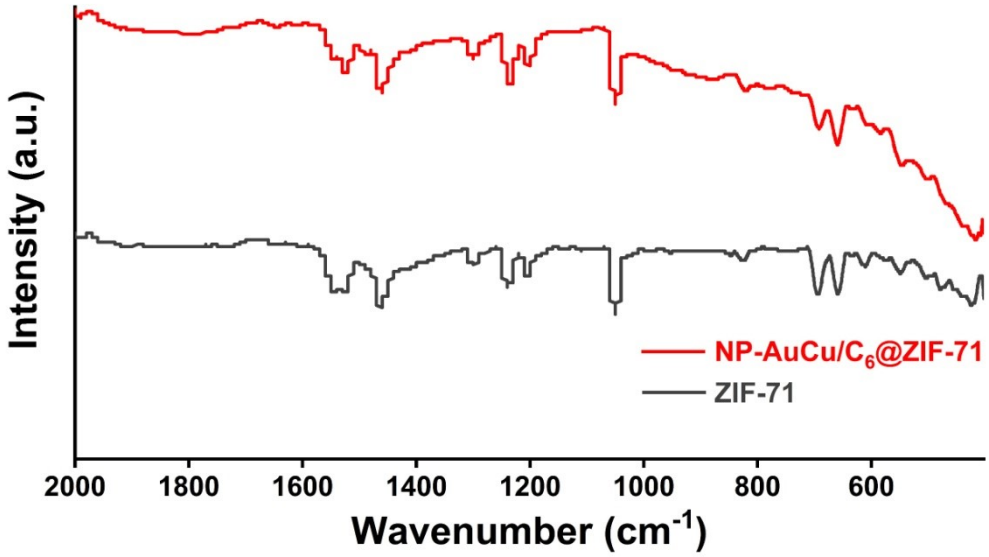

Figure S6. The infrared spectroscopy of NP-AuCu/C_6@ZIF-71 and ZIF-71.

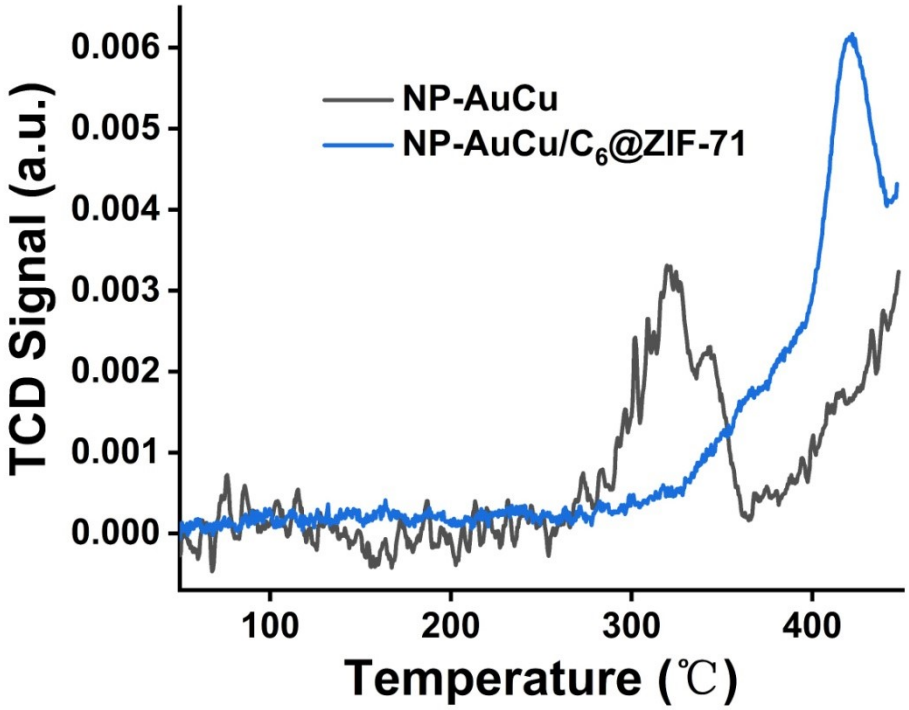

Figure S7. TPD test spectra of NP-AuCu and NP-AuCu/C_6@ZIF-71.

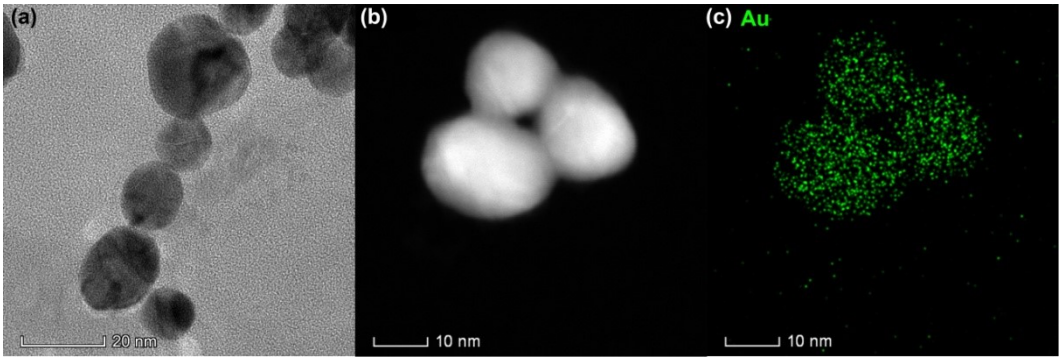

Figure S8. (a) Morphological characterization in the AuNPs in the TEM image (scale bar: 20 nm). EDS elemental mapping of (b) the AuNPs, indicating (c) Au elemental distribution (scale bar: 10 nm).

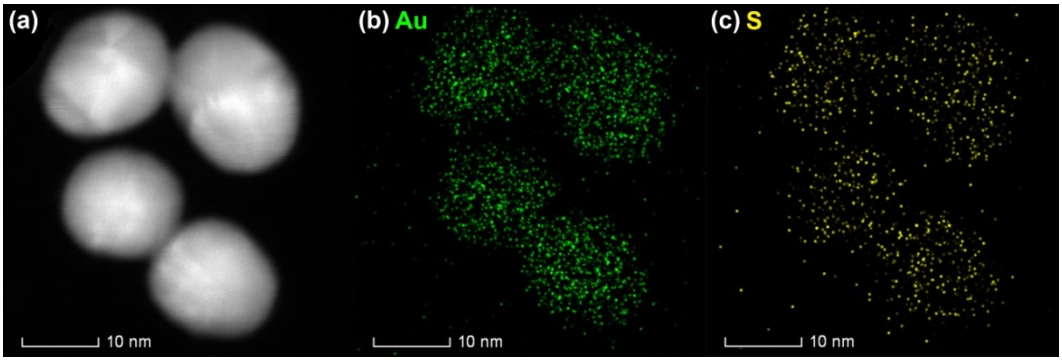

Figure S9. EDS elemental mapping of (a) the AuNPs/C_6 (scale bar: 10 nm), indicating (b) Au and (c) S elemental distribution.

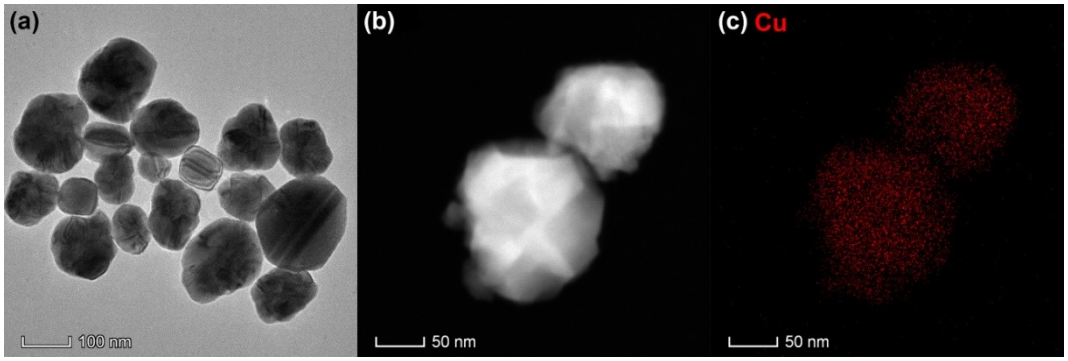

Figure S10. (a) Morphological characterization in the CuNPs in the TEM image (scale bar: 100 nm). EDS elemental mapping of (b) the CuNPs, indicating (c) Cu elemental distribution (scale bar: 50 nm).

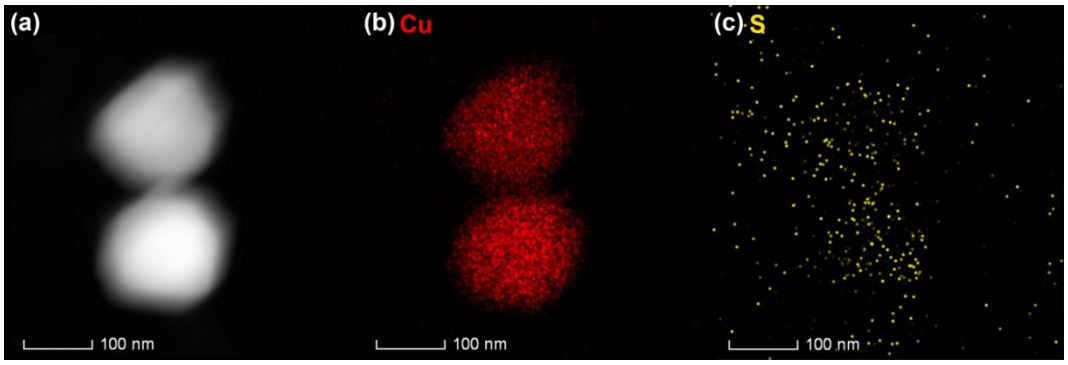

Figure S11. EDS elemental mapping of (a) the CuNPs/C_6 (scale bar: 100 nm), indicating (b) Cu and (c) S elemental distribution.

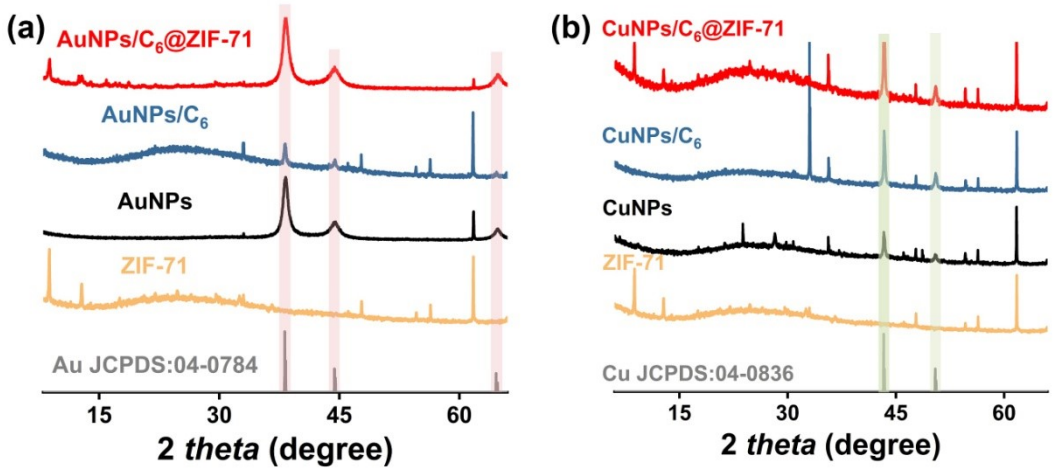

Figure S12. XRD patterns of ZIF-71, AuNPs, AuNPs/C_6, AuNPs/C_6@ZIF-71, CuNPs, CuNPs/C_6 and CuNPs/C_6@ZIF-71.

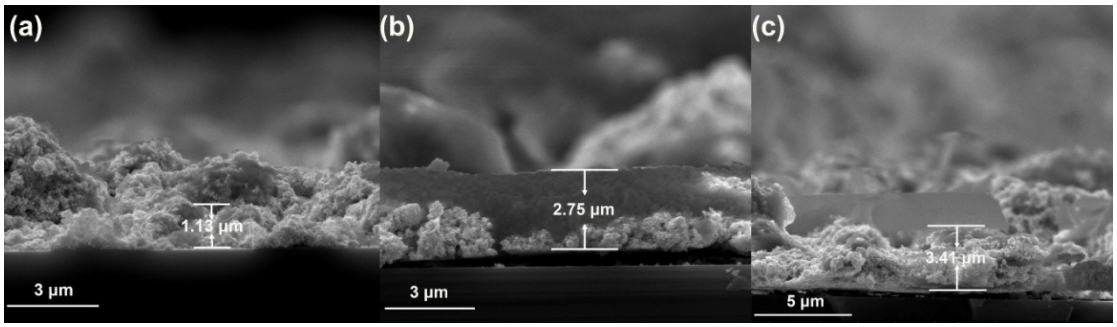

Figure S13. Cross-sectional SEM image of NP-AuCu/C_6@ZIF-71 (a) 20 minutes, (b) 80 minutes, (c) 120 minutes.

Section S3 Electrocatalysis

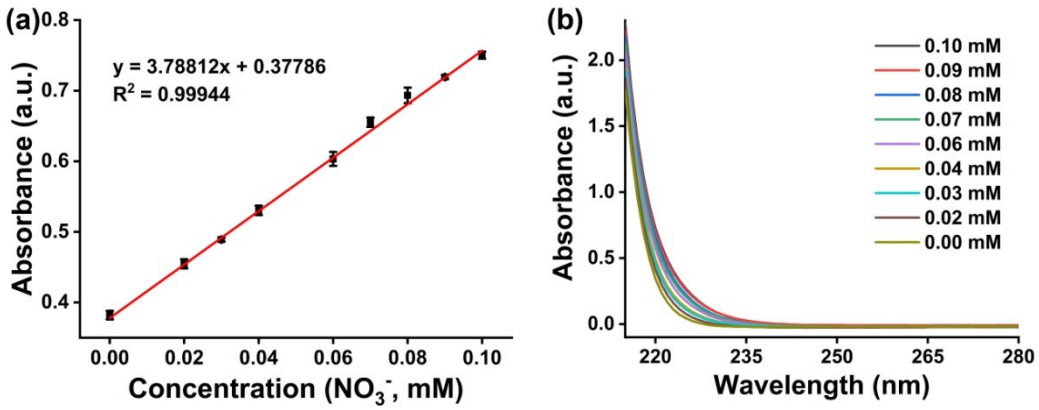

Figure S14. Calibration of UV/Vis spectrophotometry for subsequent NO_3^- quantification. (a) Linear correlation of the absorbance intensity to NO_3^- concentration (inset shows the formation of indophenol blue with different NO_3^- concentrations). (b) Absorbance spectra of UV/Vis spectrophotometry in NO_3^- solutions at various concentrations.

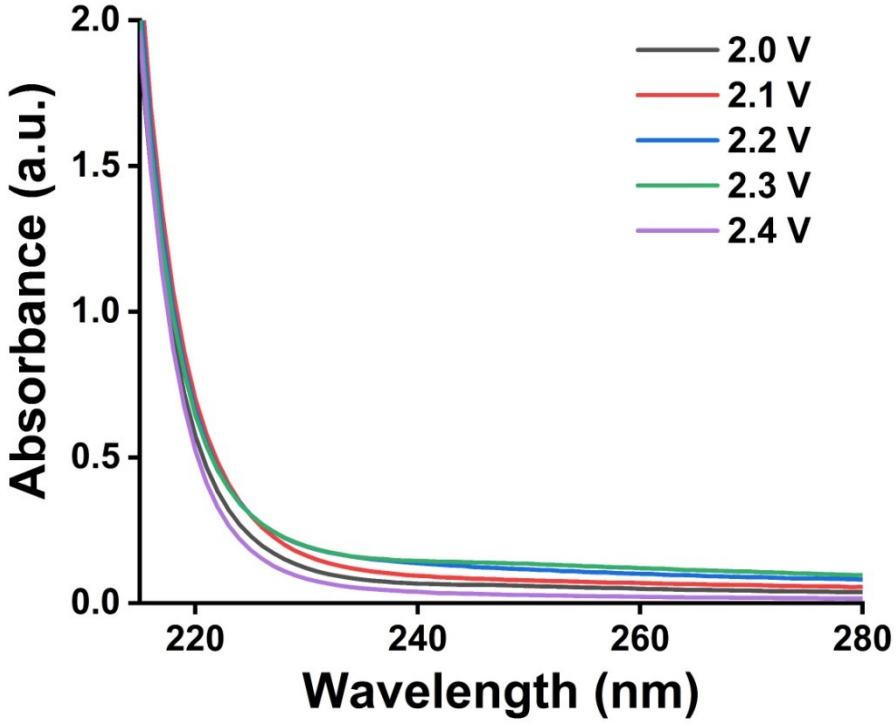

Figure S15. The concentration of NO_3^- generated in the electrolyte after 10-h of reaction was measured by UV/Vis spectrophotometry.

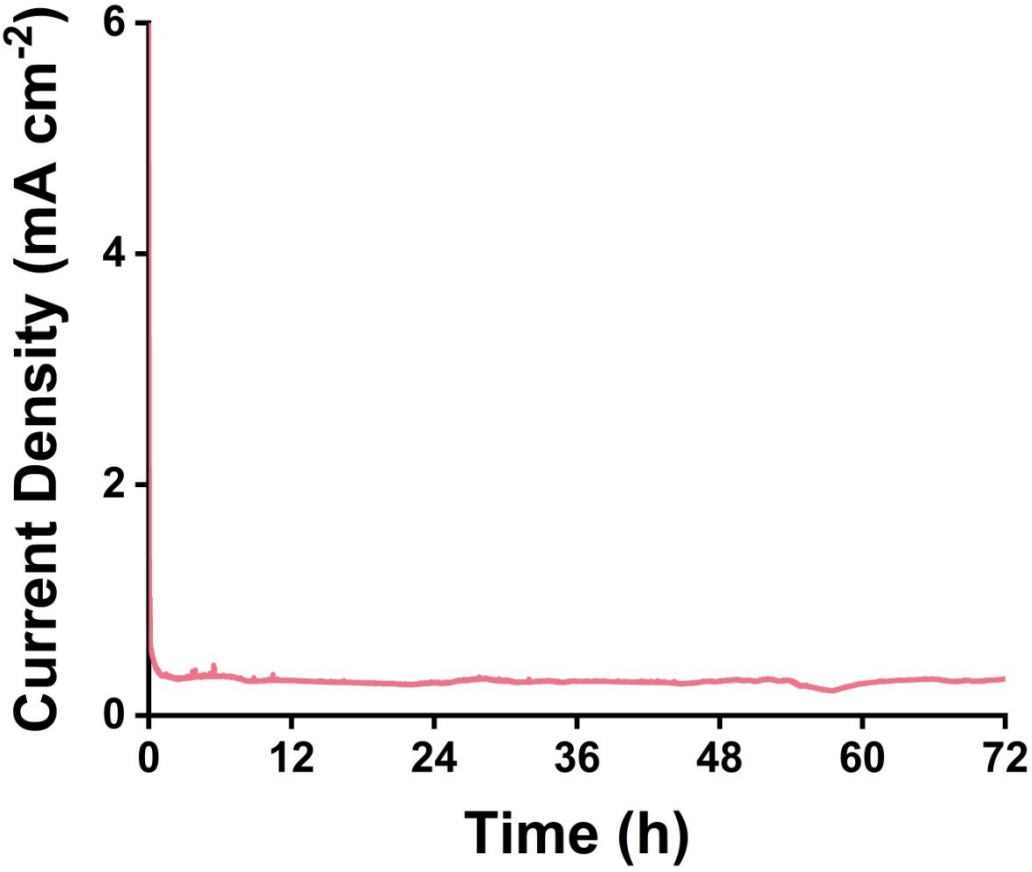

Figure S16. Time-dependent current density during electrolysis at 2.1 V vs RHE for 72 h.

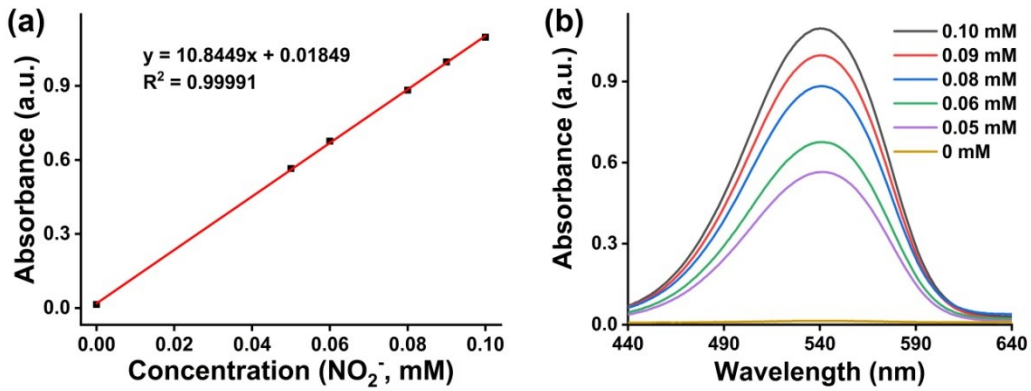

Figure S17. Calibration of UV/Vis spectrophotometry for subsequent NO_2^- quantification. (a) Linear correlation of the absorbance intensity to NO_2^- concentration (inset shows the formation of indophenol blue with different NO_2^- concentrations). (b) Absorbance spectra of UV/Vis spectrophotometry in NO_2^- solutions at various concentrations.

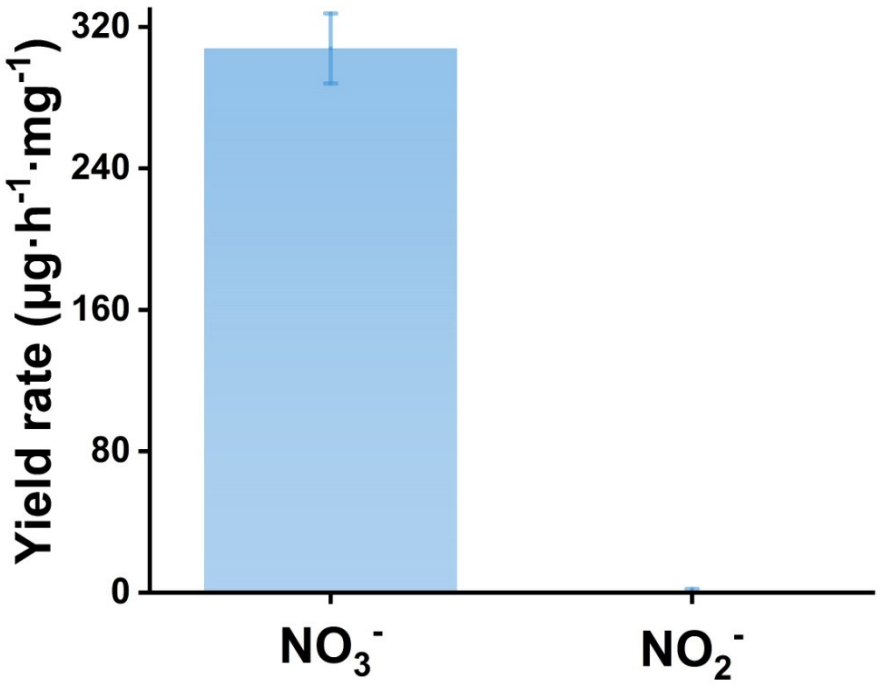

Figure S18. Yield rate for NO_3^- and NO_2^- generated during the NOR at 2.1 V vs RHE.

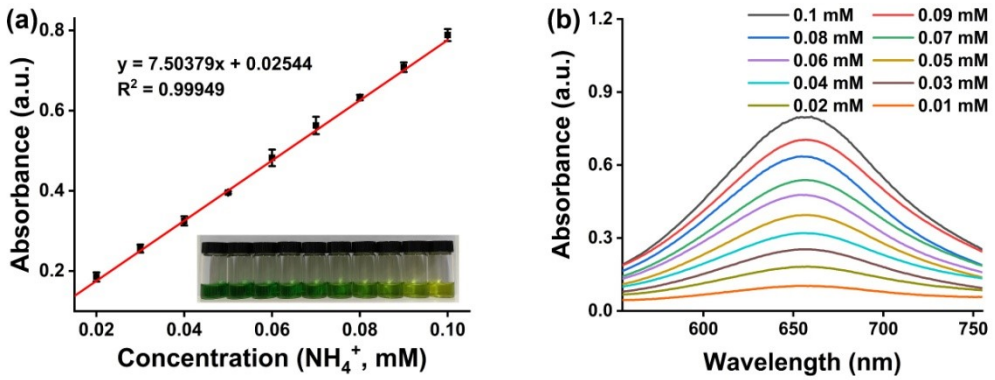

Figure S19. Calibration of the indophenol blue method for subsequent ammonia quantification. (a) Linear correlation of the absorbance intensity to NH_4^+ concentration (inset shows the formation of indophenol blue with different NH_4^+ concentrations). (b) Absorbance spectra of indophenol blue in NH_4^+ solutions at various concentrations.

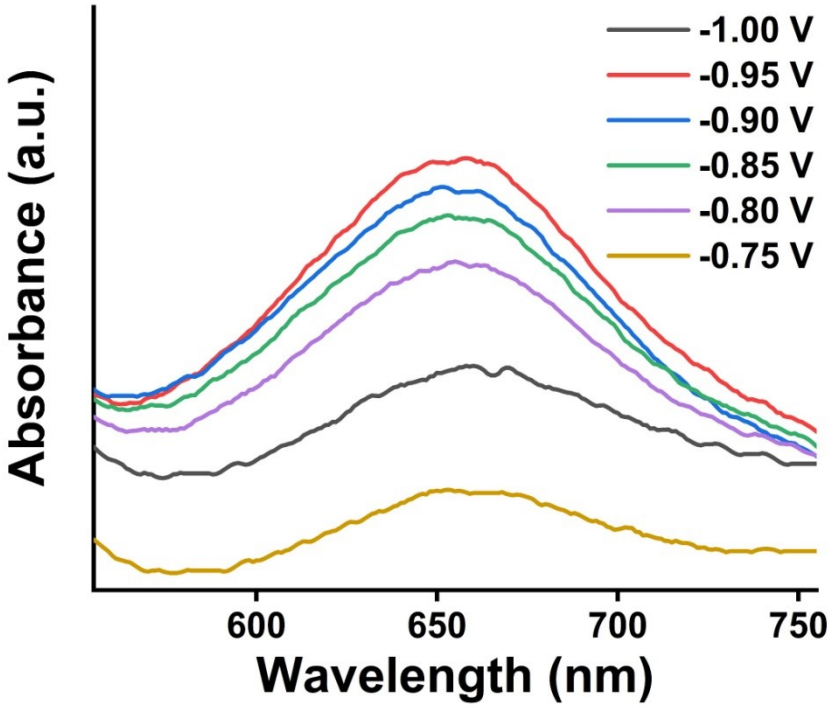

Figure S20. Corresponding UV-Vis spectra of electrolytes colored with indophenol indicator.

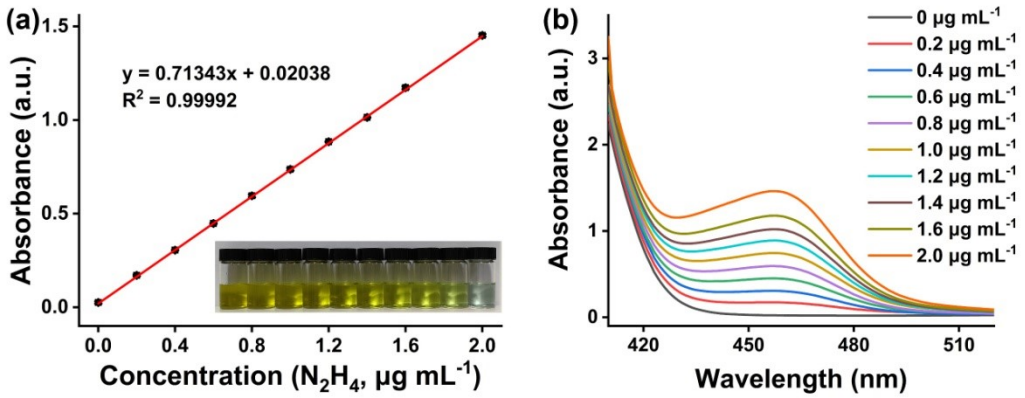

Figure S21. Calibration of the estimation method for subsequent hydrazine quantification. (a) Calibration curve used for calculation of N_2H_4 concentration. (b) Absorbance spectra of N_2H_4 solutions with various concentrations after incubated for 20 minutes at room temperature.

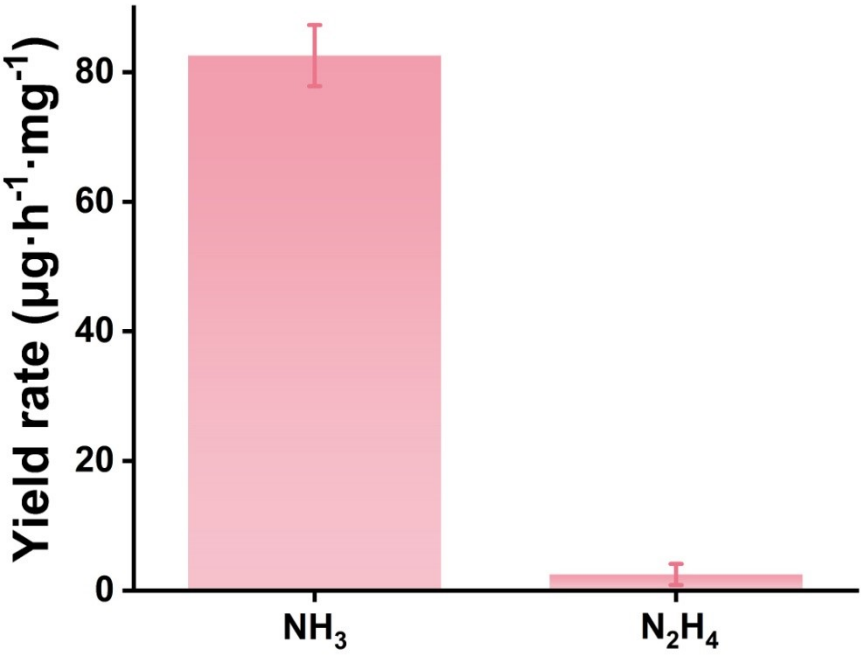

Figure S22. Yield rate for NH_3 and N_2H_4 generated during the NRR at -0.80 V vs RHE.

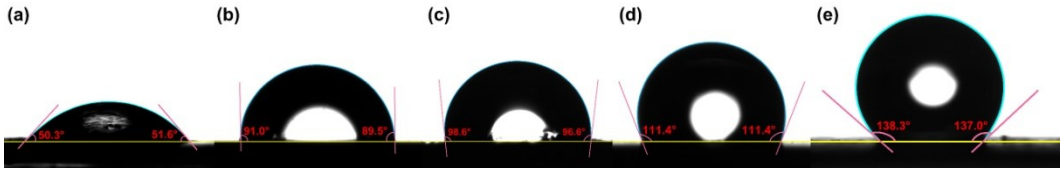

Figure S23. The static aqueous contact angle tests of (a) NP-AuCu, (b) NP-AuCu/C_6, (c) NP-AuCu/C_{12}, (d) NP-AuCu/F_{17} and (e) NP-AuCu/C_6@ZIF-71.

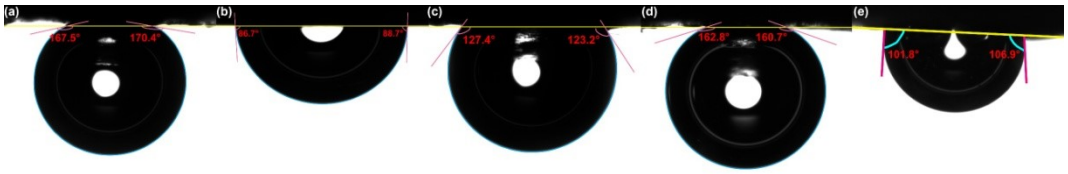

Figure S24. The nitrogen contact angle in water of (a) NP-AuCu, (b) NP-AuCu/C_6, (c) NP-AuCu/C_{12} and (d) NP-AuCu/F_{17} and (e) NP-AuCu/C_6@ZIF-71.

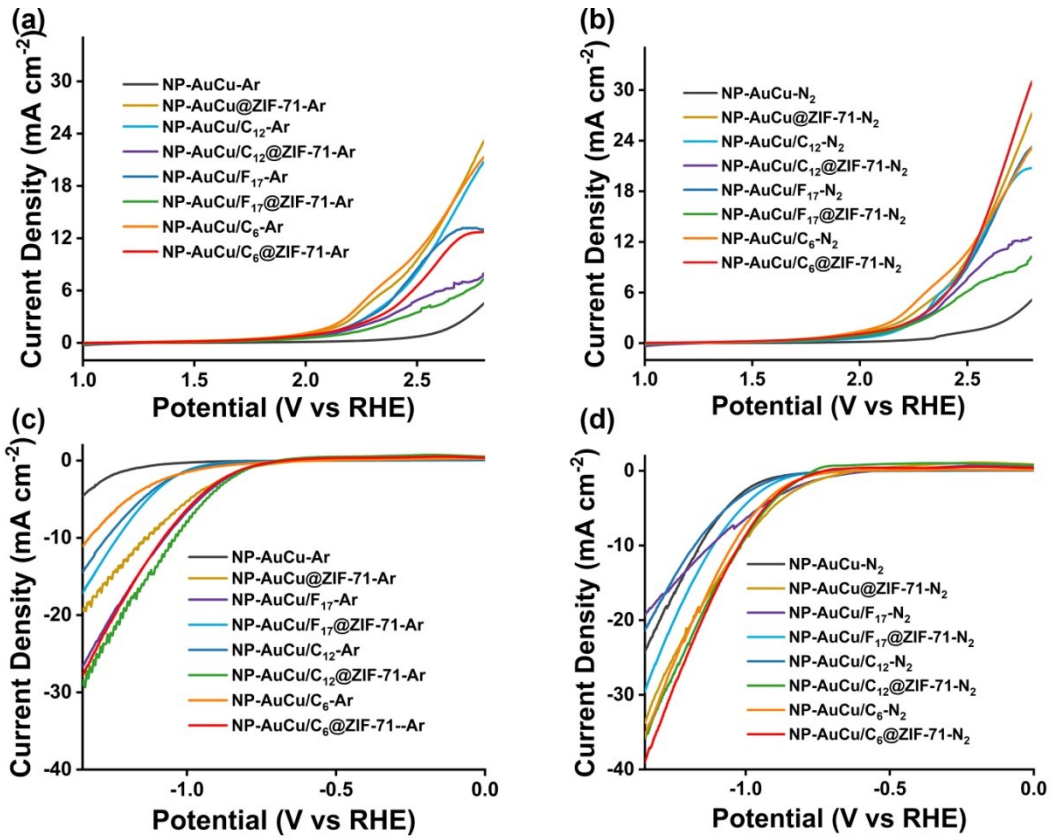

Figure S25. Linear sweep voltammetry measurements in the N_2 and Ar saturated environments, using different materials as functionalized electrodes.

Table S1. Comparison of NO_3^- yield rate, NH_3 yield rate and Faradaic efficiency of materials.

Electrode Material	NO_3^- yield rate	NH_3 yield rate	FE (%)
NP-AuCu/C_6@ZIF-71	307.89 μg·h^{-1}·mg^{-1}	82.55 μg·h^{-1}·mg^{-1}	47.79
NP-AuCu/C_6	138.37 μg·h^{-1}·mg^{-1}	73.77 μg·h^{-1}·mg^{-1}	24.37
NP-AuCu/C_{12}@ZIF-71	153.92 μg·h^{-1}·mg^{-1}	76.08 μg·h^{-1}·mg^{-1}	33.10
NP-AuCu/C_{12}	119.66 μg·h^{-1}·mg^{-1}	72.16 μg·h^{-1}·mg^{-1}	23.53
NP-AuCu/F_{17}@ZIF-71	146.57 μg·h^{-1}·mg^{-1}	70.72 μg·h^{-1}·mg^{-1}	31.53
NP-AuCu/F_{17}	109.32 μg·h^{-1}·mg^{-1}	67.38 μg·h^{-1}·mg^{-1}	19.05
NP-AuCu@ZIF-71	134.64 μg·h^{-1}·mg^{-1}	69.83 μg·h^{-1}·mg^{-1}	26.32
NP-AuCu	101.83 μg·h^{-1}·mg^{-1}	60.58 μg·h^{-1}·mg^{-1}	16.66
CuNPs/C_6@ZIF-71	105.90 μg·h^{-1}·mg^{-1}	41.13 μg·h^{-1}·mg^{-1}	23.20
CuNPs/C_6	47.71 μg·h^{-1}·mg^{-1}	30.71 μg·h^{-1}·mg^{-1}	9.73
CuNPs	29.91 μg·h^{-1}·mg^{-1}	25.20 μg·h^{-1}·mg^{-1}	5.97
AuNPs/C_6@ZIF-71	103.08 μg·h^{-1}·mg^{-1}	36.06 μg·h^{-1}·mg^{-1}	24.38
AuNPs/C_6	80.05 μg·h^{-1}·mg^{-1}	26.80 μg·h^{-1}·mg^{-1}	13.50
AuNPs	43.14 μg·h^{-1}·mg^{-1}	16.3 μg·h^{-1}·mg^{-1}	6.24
ZIF-71	25.18 μg·h^{-1}·mg^{-1}	6.71 μg·h^{-1}·mg^{-1}	5.06

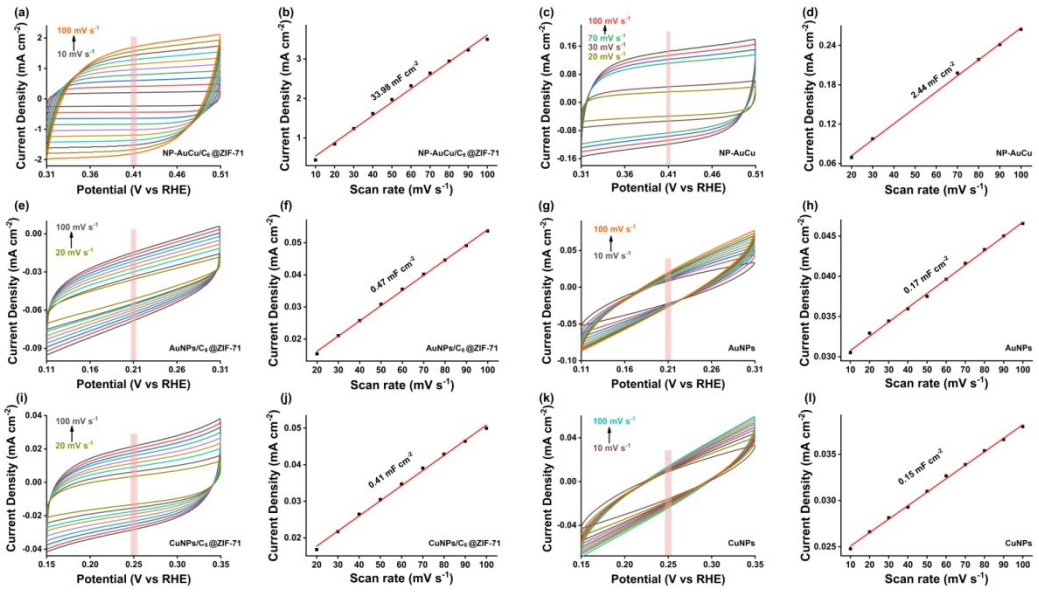

Figure S26. Cyclic voltammetry tests for synthesized (a) NP-AuCu/C_6@ZIF-71, (c) NP-AuCu, (e) AuNPs/C_6@ZIF-71, (g) AuNPs, (i) CuNPs /C_6@ZIF-71, (k) CuNPs and (b), (d), (f), (h), (j), (l) charging current density differences plotted against scan rates, respectively.

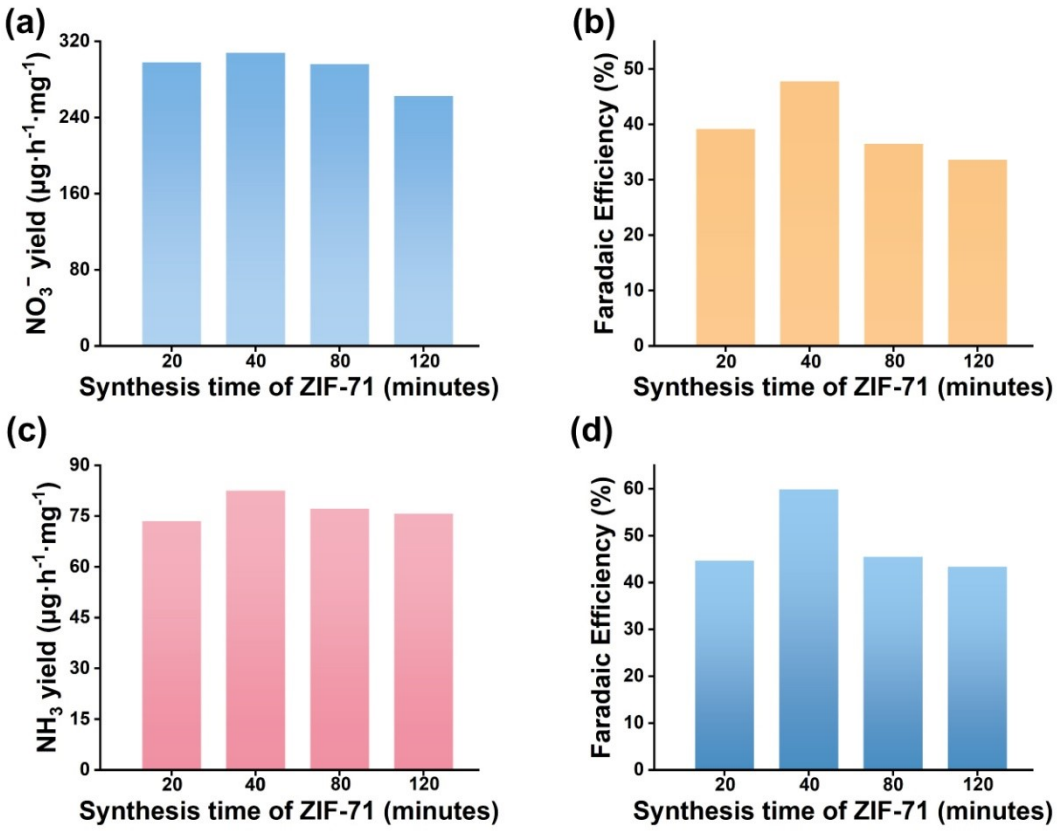

Figure S27. Corresponding NO_3^- yield rates (a) and Faradaic efficiencies of NOR (b), NH_3 yield rates (c) and Faradaic efficiencies of NRR (d) under different synthesis.

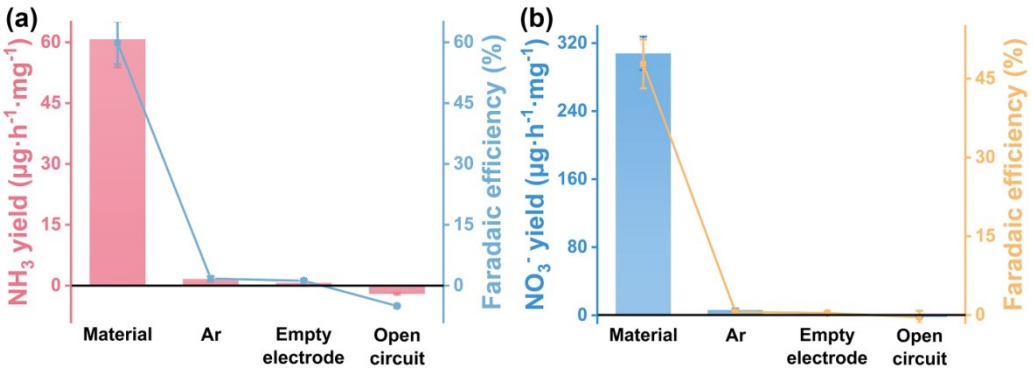

Figure S28. Faradaic efficiency of NRR, NH_3 yield rate, Faradaic efficiency of NOR and NO_3^- yield rate comparisons under different conditions.

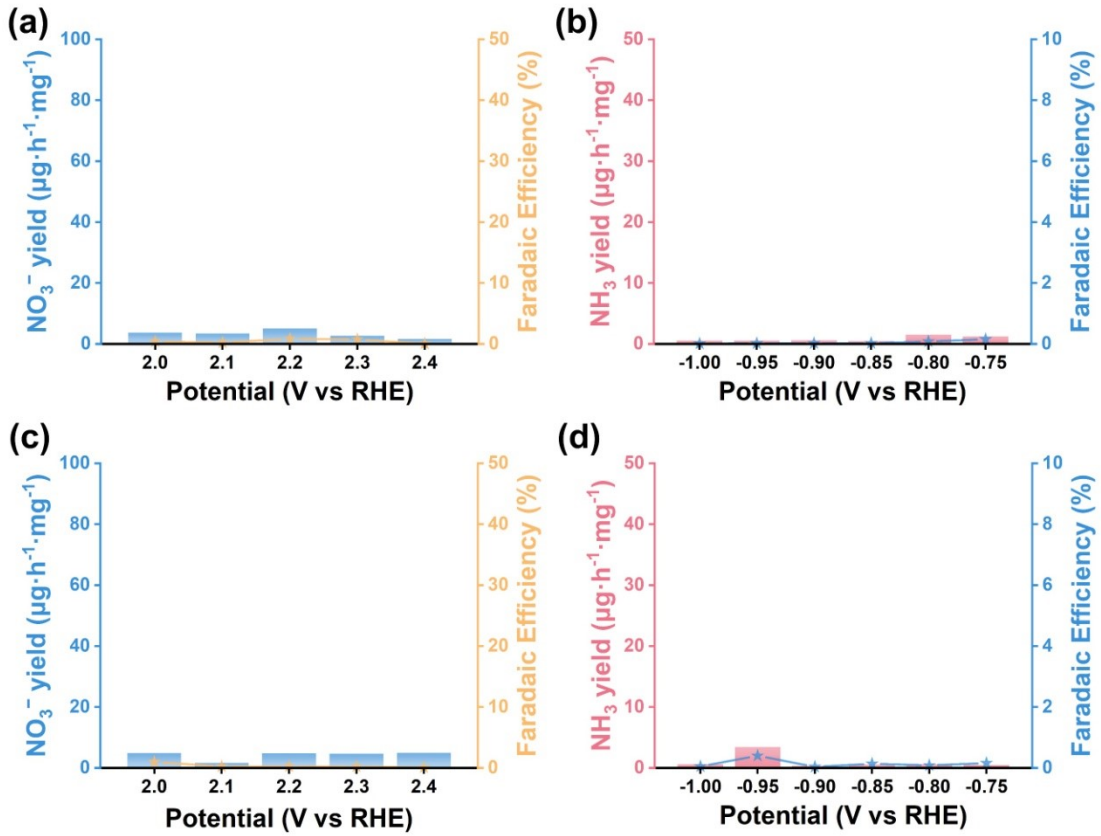

Figure S29. Corresponding NO_3^- yield rate NH_3 yield rates Faradaic efficiency of NOR and Faradaic efficiency of NRR (a, b) under Ar electrochemical condition with a series of potentials and (c, d) without applied potential under the same condition with CA tests in the Figure 2c-d and 3c-d for the comparison.

Table S2. Comparison of NO_3^- yield rate and Faradaic efficiency (FE) of materials.

Electrode Material	electrolyte	FE (%)	NO_3^- yield rate	Ref.
NP-AuCu/C_6@ZIF-71	**0.1 M KOH**	**47.79**	**307.89 μg·h^{-1}·mg^{-1}**	**This work**
$Cu_{0.5}Ni_{0.5}$/C	0.1 M Na_2SO_4	18.7	228.24 μmol h^{-1} g^{-1}	*Small*, 2023, **19**, 2301438.
Ru-HEP	0.5 M KOH	32.8	39.0 μmol mg^{-1} h^{-1}	*ACS Nano*. 2024, **18**, 17642−17650.
$Pd_{0.9}Ru_{0.1}$	0.1 M KOH	/	77.70 μmol g^{-1} h^{-1}	*ACS Catal.*, 2021, **11**, 14032.
Pb/S–TiO_2@2-MeIm/PPy/GO	0.1 M KOH	8.92	72.69 μg h^{-1} mg^{-1}	*Adv. Mater.* 2024, **36**, 2313155.
Co_3O_4 + $^{\cdot}OH$	0.1 M Na_2SO_4	20.4	89.35 μg h^{-1} mg^{-1}	*Chem. Sci.*, 2023, **14**, 1878.
$Sr_{0.9}RuO_3$	0.1 M Na_2SO_4	38.6	17.90μmol mg^{-1} h^{-1}	*Angew. Chem. Int. Ed.*, 2024, **63**, e202316097.
Ru-Mn_3O_4	0.1 M Na_2SO_4	28.87	35.34 μg h^{-1} mg^{-1}	*Adv. Mater.*, 2022, **34**, 2108180.
D-RuO_2	0.05 M H_2SO_4	6.70	767.92 μg h^{-1} mg^{-1}	*Adv. Energy Mater.*, 2023, **13**, 2300615.
Pd-s PNSs	0.1 M KOH	2.5	18.56 mg h^{-1} mg^{-1}	*Angew. Chem. Int. Ed.*, 2021, **60**, 4474.
Ce-Co_3O_4	0.1 M Na_2SO_4	31.93	24.76 μg h^{-1} mg^{-1}	*Adv. Funct. Mater.*, 2023, **33**, 2306098.

Table S3. Comparison of NH_3 yield rate and Faradaic efficiency (FE) of materials.

Electrode Material	electrolyte	FE (%)	NH_3 yield rate	Ref.
NP-AuCu/C_6@ZIF-71	**0.1 M Na_2SO_4**	**59.85**	**82.55 μg·h^{-1}·mg^{-1}**	**This work**
BMS-5	0.1 M Na_2SO_4	58.56	54.64 μg·h^{-1}·mg^{-1}	*Appl. Catal. B-Enviro.*, 2024 **355** 124173.
Rh-Mo_2C	0.05 M Na_2SO_4	15.40	26.3 μg h^{-1} cm^{-2}	*Appl. Catal. B-Environ.*, 2023, **320**, 121777.
NPG@ZIF-8	0.1 M Na_2SO_4	44	28.7 μg h^{-1} cm^{-2}	*Angew. Chem. Int. Ed.*, 2019, **58**, 15362-15366.
NC/Cr_2S_3	0.1 M Na_2SO_4	7.66	30.33 μg·h^{-1}·mg^{-1}	*Inorg. Chem. Commun.*, 2024 **168** 112869.
PdCu@UiO-S@PDMS	0.1 M HCl	13.16	20.24 μg·h^{-1}·mg^{-1}	*Adv. Mater.*, 2023, **35**, 2210669.
AuCu	0.1 M Na_2SO_4	45.70	25.70 μg h^{-1} cm^{-2}	*Chem. Commun.*, 2023, **59**, 12132.
PCuPc/O-CNT	0.01 M H_2SO_4	26.80	12.3 μg h^{-1} cm^{-2}	*ChemCatChem*, 2023, **15**, e202201631.
$FeMoS_2$/CC	1.0 M KOH	0.15%	7.81 μg h^{-1} cm^{-2}	*Energ. Fuel.*, 2023, **37**, 15967−15975.
Cu_3P@NC	0.1 M Na_2SO_4	6.3	10.40 μg·h^{-1}·mg^{-1}	*Chem. Commun.*, 2022, **58**, 2678-2681.
oxGR-NS	PBS	13.20	28.5 μg·h^{-1}·mg^{-1}	*Small* 2023, **19**, 2303221.